Inertial Vibration Damping of a Flexible Base Manipulator*

Lynnane E. GEORGE** and Wayne J. BOOK***

A rigid (micro) robot mounted serially to the tip of a long, flexible (macro) manipulator is often used to increase reach capability, but flexibility in the macromanipulator can make it susceptible to vibration. A rigid manipulator attached to a flexible but unactuated base was used to study a scheme to achieve positioning of the micromanipulator combined with enhanced vibration damping of the base. The interaction forces and torques acting between the robot and its flexible base were modeled and studied. Simulated and measured interactions generated at the base of a three degree of freedom rigid robot are compared. Simulated and experimental results are included that demonstrate with the proper control of these interactions, damping can be added to the base.

Key Words: Macro/Micromanipulator, Inertial Vibration Damping, Inertial Singularity, Flexible Manipulator, Active Vibration Control

1. Introduction

The objective of this research was to develop a combined position and enhanced vibration control scheme for a macro/micromanipulator (Fig. 1), which has long, lightweight links with a rigid robot serially attached. These are desirable for certain uses because the macromanipulator provides long reach capability while the rigid robot provides fine positioning. They are often used to perform tasks that humans may be incapable of doing or that are dangerous for humans. One application is in the nuclear industry where macro/micromanipulators are used to remove waste from underground storage tanks[1]. Another growing application is in space, where long reach capability is needed but weight is crucial[2],[3]. However, one problem with their use is that vibration is easily induced in the flexible links, either due to the movement of the robot itself or by external disturbances. The many degrees of freedom involved make control of the coupled system a complex task. This research considers the analogous problem of a rigid robot mounted to a flexible base (Fig. 2), where the base motion is due to flexibility at the tip of a macromanipulator in a fixed joint configuration.

Many researchers have addressed control schemes for macro/micromanipulators. One area involves determining trajectories that avoid inducing vibration[2],[4]; however these schemes are not useful for controlling the vibration once it occurs. The macromanipulator actuators are not the best option

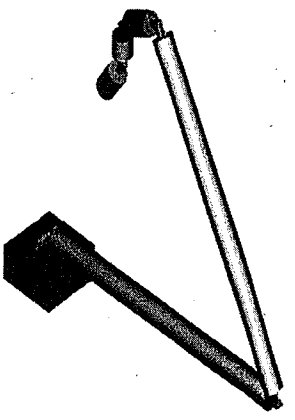

Fig. 1 Macro/Micromanipulator

* Received 22nd November, 2002 (No. 02-5193)

** Space Vehicles Directorate, US Air Force Research Laboratory, Kirtland AFB, NM. E-mail: lynnane.george@kirtland.af.mil

*** Intelligent Machine Dynamics Laboratory, George W. Woodruff School of Mechanical Engineering Georgia Institute of Technology. E-mail: wayne.book@me.gatech.edu, http://imdl.me.gatech.edu

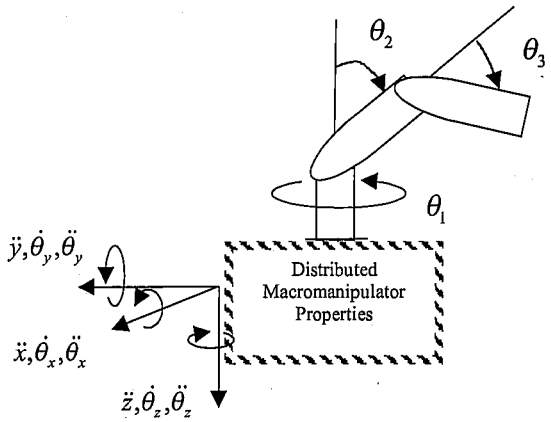

Fig. 2 Flexible base manipulator

due to the high bandwidths required and non-collocation of the actuators and the end point vibration. The use of the rigid manipulator to damp vibration in the macromanipulator has proven to be a promising area of research[1),(5),(6)]. Its motion produces interaction forces and torques, which can be applied directly to the macromanipulator. Also, the actuators can typically respond quickly and efficiently to produce large interactions. These interactions serve as disturbances under decoupled control but when controlled properly they can be used as damping forces. On the one hand, if the motion of the micromanipulator or combined system is completely prescribed by the task at hand, this method is not useful. However, under circumstances where the task will allow small movements of the rigid robot to damp the vibration, this technique can be very effective. This method requires no hardware modifications other than some type of measurement of the vibration.

2. System Model

The flexible base represents a multi-link flexible manipulator. There are many references available on modeling flexible systems[3),(7)]. Regardless of the method used, the important properties for this work are inertia (M), damping (C), and stiffness (K) estimates. It is assumed the model takes the form:

$$M(\tilde{q})\ddot{q}+C(\tilde{q})\dot{q}+K(\tilde{q})q=Q \qquad (1)$$

Since the macromanipulator's joints are locked, q represents the flexible states and consists of a finite number of modes of interest. The mass, damping, and stiffness matrices can be linearized and assumed approximately constant about an operating point, $\tilde{q}$. The interaction forces and torques generated by the rigid robot are the generalized forces, Q.

A recursive Newton-Euler method, commonly used to develop joint torque equations for rigid robots[8)], was used to find the interaction forces and torques. The elastic states of the macromanipulator affect the micromanipulator by moving its base in Cartesian space. These become boundary conditions on the first link's rotational velocities and translational and rotational accelerations, which are propagated forward to the other links. The general form of these equations is:

$$F_{IF}=B_f(\theta)\ddot{\theta}+N_f(\theta,\dot{\theta}_i\dot{\theta}_j)+C_f(\theta)\ddot{q}+N_{fc}(q,\dot{q},\theta,\dot{\theta}) \qquad (2.a)$$

$$\tau_{IF}=B_{\tau 0}(\theta)\ddot{\theta}+N_{\tau 0}(\theta,\dot{\theta}_i\dot{\theta}_j)+C_{\tau 0}(\theta)\ddot{q}+N_{\tau 0c}(q,\dot{q},\theta,\dot{\theta}) \qquad (2.b)$$

$$\tau=B_\tau(\theta)\ddot{\theta}+N_\tau(\theta,\dot{\theta}_i\dot{\theta}_j)+C_\tau(\theta)\ddot{q}+N_{\tau c}(q,\dot{q},\theta,\dot{\theta}) \qquad (2.c)$$

θ represents the rigid robot joint variables. B_f, $G_{\tau 0}$, C_f, and $C_{\tau 0}$ represent inertia effects of the micro and macro manipulators, respectively. The remaining terms represent nonlinear and gravitational effects. The third equation is the typical joint torque equation with extra coupling terms. Often actuator dynamics or other effects dominate the robot performance, so this equation could take other forms. However, it is assumed the relationship between the applied torques and joint positions is known and controllable.

3. Interactions and Inertial Singularities

The focus of this analysis was on the controllable rigid robot interactions, or those terms that are only functions of θ (the first two terms in Eqs.(2.a) and (2.b). The discussion here is primarily on the interaction forces, but the results are applicable to both forces and torques (exceptions are noted). B_f and $B_{\tau 0}$ are inertia-like matrices but they are, in general, not symmetric or positive definite (the inertia matrix for the coupled system, B_τ, is). These are important for two reasons. First, the rigid robot must have enough inertia to effectively apply interaction forces and torques to the macromanipulator. Second, there are locations in the workspace where these matrices become singular, which presents a problem since they are inverted in the control scheme. However, the more important consideration is that these "inertial singularities" represent *physical* limitations in that an inertial force or torque cannot be created in one or more degrees of freedom.

The following performance measure provides a measure of the ability of the rigid robot to generate effective interaction forces and torques and assesses its variation throughout the workspace:

$$|B_f^T(\theta)B_f(\theta)|,\ |B_{\tau 0}^T(\theta)B_{\tau 0}(\theta)| \qquad (3)$$

$B_f(\theta)$ and $B_{\tau 0}(\theta)$ will not, in general, have real eigenvalues. However, $B_f^T(\theta)B_f(\theta)$ and $B_{\tau 0}^T(\theta)B_{\tau 0}(\theta)$ will always be symmetric and have a positive determinant. Thus, the determinant, which is the product of singular values, was chosen for the performance measure and it can more easily be evaluated than

eigenvalues or singular values. This measure not only provides a measure of how these effects vary throughout the workspace, but also shows regions where full multi-DOF inertial damping capability is not possible. The goal here is to use this performance measure to choose robot joint space configurations where the inertia effects are large, whenever possible. Alternately the combined ability of the robot to generate interaction forces and torques may be evaluated by assessing:

$$|B^T(\theta)B(\theta)|$$

where:

$$B(\theta)=\begin{bmatrix} B_f(\theta) \\ B_{\tau 0}(\theta) \end{bmatrix} \qquad (4)$$

As an example, consider a three degree of freedom anthropomorphic robot (shown in Fig. 2). By considering the force performance measure of Eq. (3), a few important features become apparent (Fig. 3). These singularities consist of some of the kinematic singularities plus additional dynamically singular configurations.

These are driven by the columns of B_f when the matrix contains:

1) Linearly dependent columns, which indicate that the inertia forces created by two or more links are parallel. For the anthropomorphic robot this scenario occurs when the last two links are aligned. This also corresponds to a kinematic singularity, when the velocities generated by the two links are parallel. These are not a major concern since these would not be normal operating regions.

2) A column of zeros, which indicates a location in the workspace where the motion of a joint cannot create any inertia interaction forces. This occurs when the system center of mass is aligned along an axis of rotation. These inertial singularities depend on the location of the center of mass of the system. Note the interaction force and torque performance is driven by the joint space configuration of the robot.

The nonlinear rigid robot effects (N_f, $N_{\tau 0}$) may become significant in certain workspace regions. However, with the proper choice of vibration control feedback gains, the amplitude of the commanded joint motion can be limited to ensure the inertia effects remain dominant. Under these conditions, the nonlinear and gravitational effects can be linearized about an operating point. Thus, the most important dynamics take the form:

$$\begin{bmatrix} M_f+A_f(\theta) & B_{11f}(\theta) & B_f(\theta) \\ A_{\tau 0}(\theta) & J+B_{11\tau 0}(\theta) & B_{\tau 0}(\theta) \\ B_f^T(\theta) & B_{\tau 0}^T(\theta) & B_\tau(\theta) \end{bmatrix} \begin{bmatrix} \ddot{x}_f \\ \ddot{\theta}_f \\ \ddot{\theta} \end{bmatrix} + \begin{bmatrix} C & 0 & 0 \\ 0 & C_\tau & 0 \\ 0 & 0 & 0 \end{bmatrix} \begin{bmatrix} \dot{x}_f \\ \dot{\theta}_f \\ \dot{\theta} \end{bmatrix} + \begin{bmatrix} K & 0 & 0 \\ 0 & K_\tau & 0 \\ 0 & 0 & 0 \end{bmatrix} \begin{bmatrix} x_f \\ \theta_f \\ \theta \end{bmatrix} = \begin{bmatrix} 0 \\ 0 \\ \tau \end{bmatrix} \qquad (5)$$

Here the translational (x_f) and rotational (θ_f) flexible dynamics are summations of the flexible states, q, as defined in Eq. (1).

Nonlinear effects

This section investigates the nonlinear interaction forces and torques expected during multi-degree of freedom inertial damping. Assuming harmonic base vibration of mode i of the flexible base, the base motion and prescribed interaction forces and torques will be harmonic (discussed in section 5). The variation of the nonlinear centrifugal and coriolis forces can be seen in Fig. 4. There are several important points to be made. First, the magnitude of the nonlinear forces is relatively small. In addition, the coriolis forces are largest in regions of poor inertia performance (case 2); operation in these regions can be avoided by using the performance measure given by Eqs. (3) and (4). However, the centrifugal forces become largest around kinematic singularity regions (case 1). Operation around these regions may be necessary (for torques, coriolis effects are more of a concern).

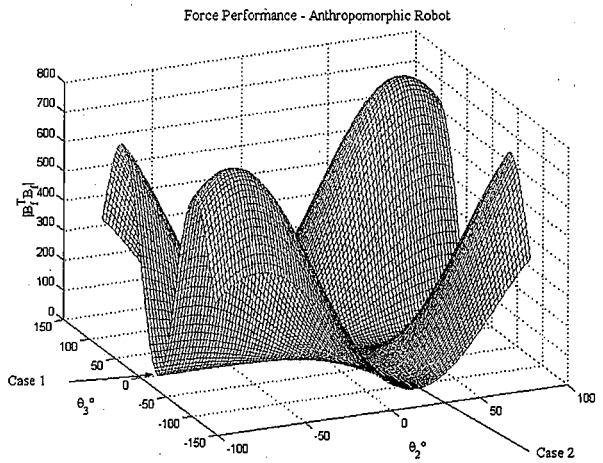

Fig. 3 Variation of anthropomorphic interaction forces

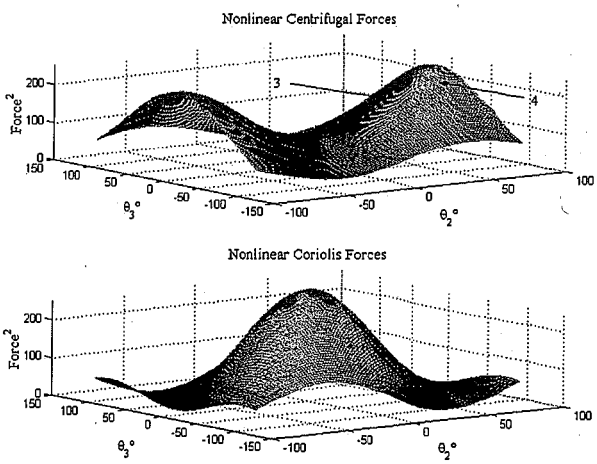

Fig. 4 Variation of nonlinear forces

These points were further investigated by simulating the interactions due to harmonic motion of a three link anthropomorphic robot. As can be seen in Fig. 5, in a workspace region (labeled 3 in Fig. 4) where the inertia effects are predicted to be large, [0°, 70°, 70°], the ratio of the inertia to nonlinear forces is large (inertia and total force traces are nearly overlaid). However, this ratio becomes poorer when the centrifugal forces become larger at [0°, 70°, −10°] (labeled 4). In this case, the inertia forces act primarily in the x direction (as defined in Fig. 2), while the centrifugal forces are all aligned primarily in the y direction. The ratios in the x and z directions are large and not shown here.

Some general conclusions can be made about the interaction effects, which will be used to develop the vibration controller discussed later:

1) The nonlinear and inertia effects are driven by two factors: the configuration of the robot and its joint accelerations and velocities. The inertia performance measure of Eqs. (3) and (4) can be used to choose inverse kinematic solution(s) best suited for inertial damping. As an example, consider the anthropomorphic robot in Fig. 6. This figure represents a macromanipulator (first two links) with the three link rigid anthropomorphic robot mounted serially to its tip. The rigid robot in the configuration on the right is much better at inertial damping than it is in the configuration on the left. In the configuration on the left, the robot is essentially unable to damp vibration in the out-of-page direction. Since the CG of the robot is along the axis of rotation of joint one, its motion will not create inertial forces. This corresponds to a case 2 inertial singularity shown in Fig. 3. The configuration on the right shows the robot in a much better configuration corresponding with the peak at the front of the plot.

2) In general, the inertia effects are dominant but there are configurations where the nonlinear effects can become large. The inertia effects are functions of the joint accelerations while the nonlinear effects are functions of the joint velocities. The amplitude of joint motion directly influences the ratio of joint accelerations to velocities. The relationship between the joint amplitudes and feedback gains will be discussed later and gain limits established to ensure this ratio remains favorable for inertial damping.

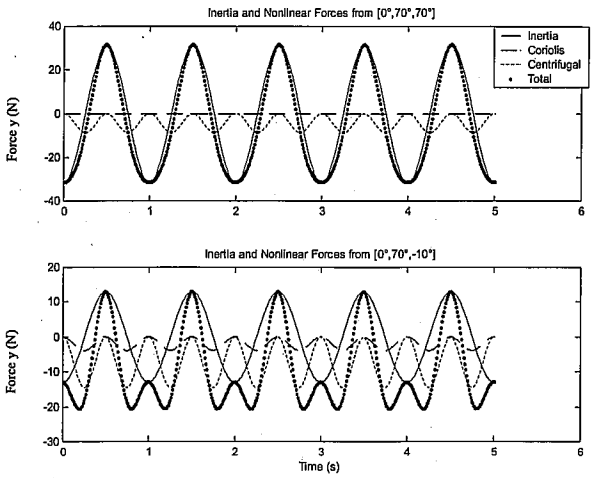

Fig. 5 Variation of nonlinear forces

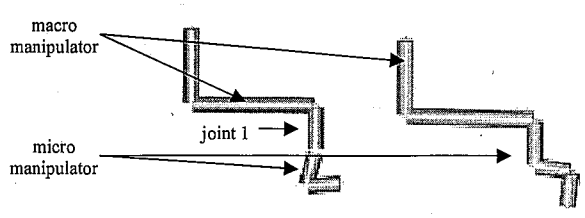

Fig. 6 Alternate inverse kinematic configurations

4. Force/Torque Verification Testing

The ability of the method presented in section 2 to predict the interaction forces and torques and simulation results discussed in the previous section were verified experimentally. The testbed consists of a three degree of freedom anthropomorphic robot mounted to the base of a flexible link, as shown in Fig. 7. A six-axis ATI force/torque sensor was mounted between the robot and its flexible base and it was braced to isolate the effects due to only the rigid robot. Sinusoidal inputs were sent to each joint individually as well as simultaneously and the interaction forces and torques recorded. Test results verified inertia effects dominate the interactions when the robot is in a configuration with large predicted iner-

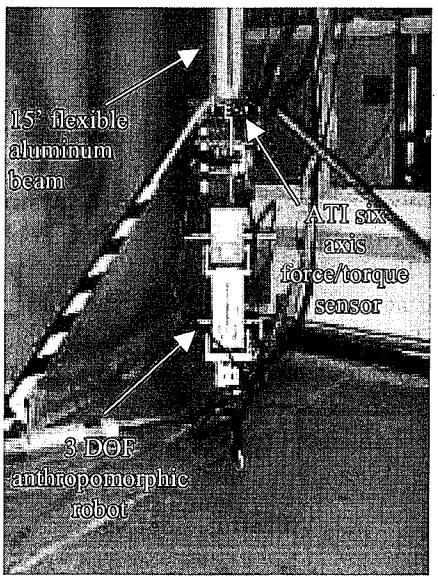

Fig. 7 Georgia tech testbed

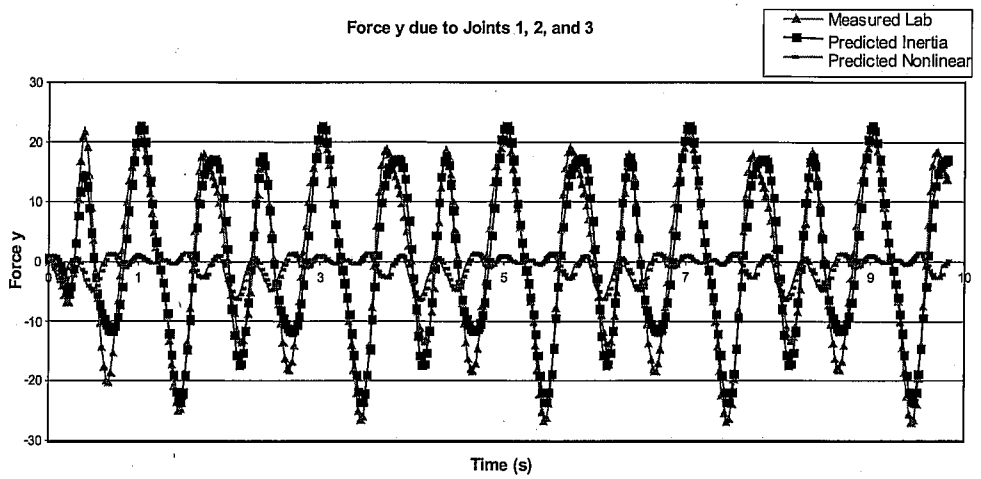

Fig. 8 Predicted and measured interaction forces at [45°, 45°, 60°]

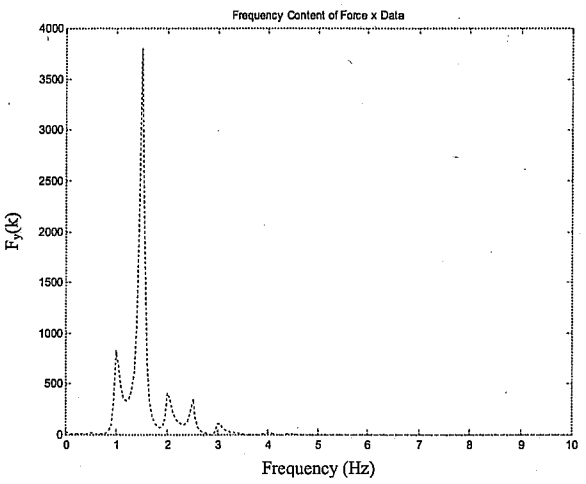

Fig. 9 Frequency content of force data

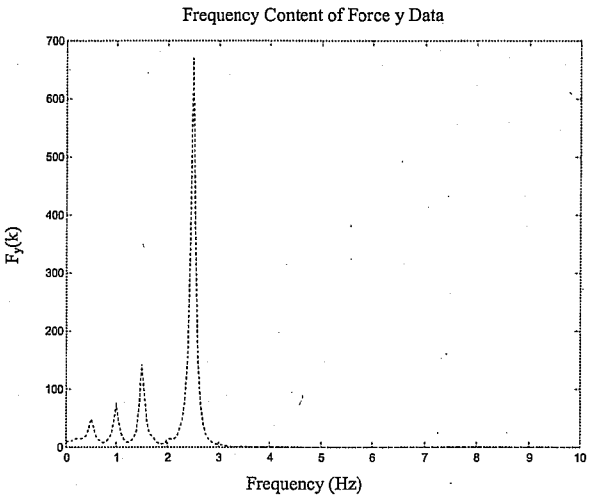

Fig. 10 Frequency content of force data due to joints 1 and 2 actuating near an inertial singularity

tia/nonlinear effect ratios. One representative example is shown in Fig. 8. In this test, all three joints are actuating harmonically at 1, 1.5, and 2 Hz, respectively. The frequency content of this data can be seen in Fig. 9. The fundamental frequencies are largest while some higher harmonics are also noticeable at 2.5 and 3 Hz.

However, in other workspace regions nonlinear effects become much more notable, as can be seen in Fig. 10. In this case, two joints of the robot are actuating at 1 and 1.5 Hz near an inertial singularity region. The coriolis force at 2.5 Hz (combination of fundamental frequencies) is clearly a problem. More examples may be found in Ref.(9). One important note is that the amplitude of motion (controllable by the feedback gains) has not yet been considered.

5. Vibration Controller

The goal of this section is to describe the vibration controller and establish a range of feedback gains to ensure vibration energy is removed from the system. This includes establishing gain limits that constrain the rigid robot joint amplitudes so the interactions (inertia effects) due to joint accelerations are greater than those due to joint velocities (nonlinear effects). The overall control schematic is shown in Fig. 11.

First, a performance index was developed to predict the effectiveness of the inertial damping control scheme. The variation in inertia performance, discussed in section 3, only varies with the joint configuration of the robot. Hence, it may be used to choose the best inverse kinematic solution(s) for inertial damping. The discussion included here only addresses the rigid robot inertia effects. However, the performance index, discussed in more detail in Ref. (9), includes other effects such as the macromanipulator and micromanipulator inertias and limits on allowable joint accelerations.

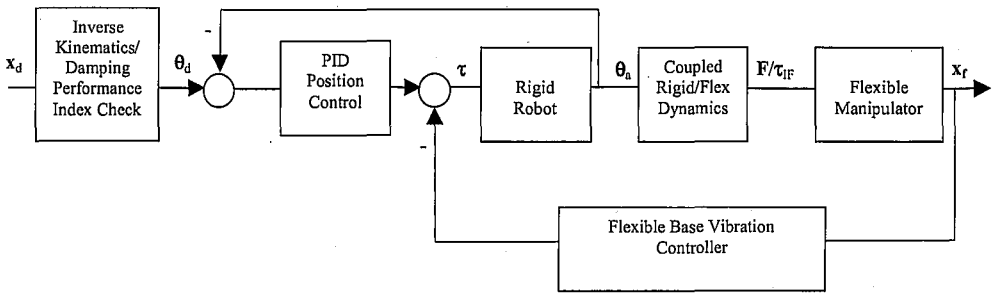

Fig. 11 Combined position/vibration controller

The flexible manipulator is modeled by Eq.(1), the coupled rigid/flex dynamics by Eqs.(2.a) and (2.b), and the rigid robot model by Eq.(2.c). Assuming the robot is not operating about a singularity point, the vibration controller prescribes the joint accelerations out of phase with the base velocity as follows:

$$\ddot{\boldsymbol{\theta}} = -ID(\boldsymbol{\theta}, \dot{\boldsymbol{\theta}})\boldsymbol{K}\dot{\boldsymbol{x}}_f \tag{6}$$

ID is an inverse dynamics function designed to cancel the significant rigid robot dynamics. It is found by solving Eq.(2.c) for $\ddot{\boldsymbol{\theta}}$ and substituting the resulting expression in Eqs.(2.a) and (2.b). The resulting expression is lengthy, but with the limits on gains discussed later, the inertia effects are most significant and the interactions may be approximated by:

$$\boldsymbol{F}_{IF} \approx B_f(\boldsymbol{\theta})\boldsymbol{B}_\tau^{-1}(\boldsymbol{\theta})\boldsymbol{\tau}$$
$$\boldsymbol{\tau}_{IF} \approx B_{\tau 0}(\boldsymbol{\theta})\boldsymbol{B}_\tau^{-1}(\boldsymbol{\theta})\boldsymbol{\tau} \tag{7}$$

The inverse dynamics function then inverts these functions so the applied torque may be commanded to provide the desired interaction forces and torques. $\boldsymbol{K}$ is a diagonal matrix of gains K_i, where K_i is the gain for the ith vibrational degree of freedom. Thus, the prescribed joint accelerations will be:

$$\ddot{\boldsymbol{\theta}} = -B^{-1}(\boldsymbol{\theta})\boldsymbol{K}\dot{\boldsymbol{x}}_f \tag{8}$$

$B^{-1}(\boldsymbol{\theta})$ will exist whenever $B(\boldsymbol{\theta})$ is non-singular. When the matrix is singular, the robot loses its ability to create effective interactions in one or more degrees of freedom.

However, the joint torques will need to be commanded so the final vibration controller takes the form:

$$\boldsymbol{\tau} = -B_\tau(\boldsymbol{\theta})B^{-1}(\boldsymbol{\theta})\boldsymbol{K}\dot{\boldsymbol{x}}_f \tag{9}$$

$B_\tau(\boldsymbol{\theta})$ and $B(\boldsymbol{\theta})$ were defined in Eqs.(2) and (4). Now the desired interactions can be controlled out of phase with the base velocity, providing damping to the flexible base. It is assumed the rigid joint positions, $\boldsymbol{\theta}$, are measured and available for use in the control scheme. There should be a minimum value established for the determinant of the inertia matrix to prevent it from being inverted when the robot is passing through a singularity configuration. Although these regions will be avoided for point-to-point motion and fixed configuration operations, it may be necessary to pass through the singularity regions and limit the controller output during these transitions.

It is assumed the PID position controller is designed separately for rigid robot control. The control scheme takes advantage of the fact that the base vibration is of relatively high frequency compared to the rigid robot motion required to perform a task. The separation of bandwidths, or time constants, between the position and vibration control loops allows them to be considered separately. This is not addressed further here, but more details can be found in Ref.(10). When this is the case, increasing vibration feedback gains, $\boldsymbol{K}$, results in a direct increase in macromanipulator damping. However, it is important to check the validity of this assumption for the specific application.

Assuming harmonic base vibration of mode i, the base motion and prescribed joint accelerations and velocities will be harmonic and take the form:

$$x_i = X_i \sin \omega_i t$$
$$\ddot{\boldsymbol{\theta}}_j = -B^{-1}(\tilde{\boldsymbol{\theta}})K_i X_i \omega_i \cos \omega_i t$$
$$\dot{\boldsymbol{\theta}}_j = -B^{-1}(\tilde{\boldsymbol{\theta}})K_i X_i \sin \omega_i t \tag{10}$$

It is assumed the inertia matrix, $B(\boldsymbol{\theta})$, can be linearized and is approximately constant about an operating point. The feedback gains will be selected to ensure this is a reasonable assumption. The maximum amplitude of joint motion, A, will occur during the first few cycles of vibration damping and for each joint can be written as:

$$|\theta_j| = \frac{K_i B(\tilde{\boldsymbol{\theta}})^{-1} X_i}{\omega_i} \equiv A \tag{11}$$

It is clear that an upper limit on the feedback gains is necessary. One reason is that there will be physical limits on the range of motion of the robot. Another reason could be that actuators may have saturation limits, so some realistic limits on gains will have to be established to avoid actuator saturation. Yet another consideration is the ratio of the inertia forces (functions of the joint accelerations), to the nonlinear forces (functions of the joint velocities). The centrifugal effects become functions of the square of the joint velocities. Solving Eq.(11) for K_i and substituting into 10 yields:

$$\frac{|\ddot{\theta}_j|}{|\dot{\theta}_j^2|}=\frac{A\omega_i^2}{A^2\omega_i^2}=\frac{1}{A} \tag{12}$$

Likewise, the ratio of inertia to coriolis effects takes the form:

$$\frac{|\ddot{\theta}_j|}{|\dot{\theta}_i\dot{\theta}_j|}=\frac{\omega_i}{A_j\omega_j} \tag{13}$$

Notice by relating the feedback gains to the amplitude of joint motion, the ratios become inversely proportional to the amplitude of motion. Thus, A can be limited to ensure the joint acceleration effects remain larger than the joint velocity effects. One upper limit is $A<1$ radian, although there may be more restrictive limits due to other considerations. The gains should be limited such that:

$$K_i<\frac{\omega_{i\,\min}B(\tilde{\theta})_{\min}}{X_{i\,\max}}A \tag{14}$$

The true multi degree-of-freedom case is more complex, of course. The selection of A and $B_{\min}$ will be specific to the macro/micromanipulator. However, the above limit will help reduce the significance of the nonlinear effects, even when in workspace locations where they can become large. Also note this ratio improves with decreasing amplitude, which increases the effectiveness of the scheme as the vibration is damped. A rule of thumb that appears to work well for the anthropomorphic robot considered in simulation and experiments is $A=B_{\min}=1$. If this is too restrictive, a more exact determination of acceptable $B_{\min}$ and maximum amplitudes may be necessary.

Nevertheless, the nonlinear forces will still be commanded along with the damping forces. The lower limit on the control gains was established by considering a worst-case scenario where the nonlinear effects directly excite a mode of the flexible system. The goal here is to ensure net energy removal from the system. This is not discussed further here, but details may be found in Ref.(9). Limiting the gains to the range:

$$0<K_i<\frac{\omega_{i,\,\min}B(\tilde{\theta})_{\min}}{X_{i,\,\max}}A \tag{15}$$

will ensure effects due to joint accelerations are greater than those due to joint velocities. It will also ensure there is enough damping available for higher modes of vibration (if a concern) to remove vibration energy if they are excited.

6. Simulations

Simulations were created in Matlab Simulink for a three degree of freedom anthropomorphic robot mounted on a flexible base. The configuration is similar to the Georgia Tech testbed shown in Fig. 7 (without the braces). Two modes of transverse vibration were assumed in each planar direction and one torsional mode to allow up to five degrees of freedom of vibration. This yielded the mass and stiffness properties; structural damping estimates were determined from modal testing. The resulting equations of motion take the form of Eq.(1) with constant matrices. The rigid robot was modeled using the Newton-Euler method described previously. The rigid robot and flex/rigid robot dynamic models include both inertia and nonlinear rigid robot terms (N_f, N_{r0}, and N_r) in order to ensure assumptions made regarding the dominance of the inertia effects are valid. The fundamental modes of the x and y directions were chosen at 1.4 Hz (x) and 1.8 Hz (y), approximately those observed on the experimental testbed, while the higher modes and torsional modes were estimated from beam theory.

Simulations were developed to verify that, with the proper selection of feedback control gains, the controller could successfully damp all modes of base vibration due to an applied disturbance or robot motion. The simulation results included here focus on the use of the performance index to predict damping performance. Point-to-point rigid robot motion was commanded to simulate the end effector moving to four corners of a square. The performance index was used to choose the best inverse kinematics track for inertial damping. The two trajectories are shown in Table 1.

The resulting joint motion and base vibration can be seen in Figs. 12 and 13. The comparisons are with vibration control using the inverse kinematics path preferable for inertial damping (Traj. 2) and using the alternate path (Traj. 1) with and without vibration control. Note the other two inverse dynamics solutions yield identical results since for the anthropomorphic robot the damping performance only varies with the configuration of joints 2 and 3. The obvious tradeoff is that the joint position is affected when under inertial damping control, as can be seen in Fig. 12. This is especially pronounced at the beginning and end of each leg, which is expected since the joint accelerations are largest when the robot starts and stops. The motion, however, is used to quickly damp the vibration. The other tradeoff is the increased amplitude of

Table 1 Simulated trajectory parameters

End Point (m)	4 .4 .4	-.2 .4 .4	-.2 -.2 .4	.4 -.2 .4	.4 .4 .4
Traj 1 θ_1 (rad)	.785	2.04	-2.36	-.471	.785
θ_2 (rad)	1.48	1.57	1.54	1.57	1.48
θ_3 (rad)	1.05	1.45	1.82	1.45	1.05
Traj 2 θ_1 (rad)	.785	2.04	-2.36	-.471	.785
θ_2 (rad)	.436	.122	-.297	.122	.436
θ_3 (rad)	-1.05	-1.45	-1.83	-1.45	-1.05
Time (s)	0-1	5-21	25-41	45-61	65-80

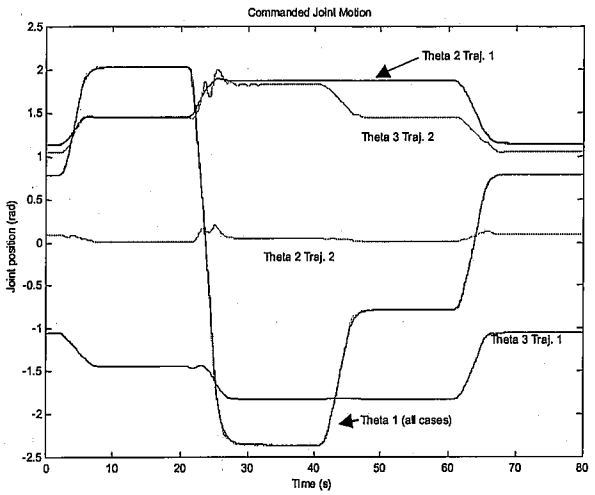

Fig. 12 Simulated point-to-point joint motion

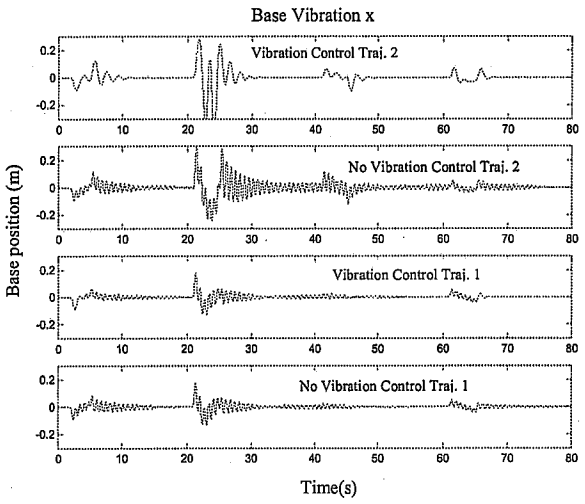

Fig. 13 Simulated base vibration due to rigid robot motion

vibration induced by moving into the better joint configurations. Compare the amplitude of the base vibration in the top and third plots in Fig. 13. The amplitude in the top figure is larger because the configuration allows more coupling between the robot and its base, thus the motion of the robot creates larger disturbances in the base. However, these configurations also allows more effective coupling to damp the vibration more quickly, while the alternate track is much less effective.

Another interesting phenomenon that occurs in non-linear multi-degree of freedom damping simulations is that there is a limit on the maximum damping available. An upper limit on gains was established by Eq. (15) simulations and experiments verified that this limit should be carefully adhered to. However, the exact determination of the specific parameters is challenging. When operating in the range, an increase in feedback gain $\boldsymbol{K}$ results in an increase in damping.

Table 2 Active damping controller disturbance rejection

Disturbance Applied	Mode (Hz)	Detected Primarily in Direction	ζ	% Improvement
x	1	x	.0239	28.5
x	1.2	y,z	.0392	485.1
x	2	x,y,z	.0231	-----
x	4.2	x,z	.0164	88.5
y	1	x,z	.0499	168.3
y	1.2	y,z	.0332	395.5
y	4.2	x,z	.0111	27.6
y	7	y,z	.0132	157.3
y	9	y,z	.0081	188.3
z	1	x	.0311	67.2
z	1.2	y,z	.0419	525.3
z	4	x,z	.0163	87.4
z	7	y,z	.0166	224.6
z	9	y,z	.0082	191.8
General	1	x	.0256	37.6
General	1.2	y,z	.0359	435.8
General	4.2	x,z	.0120	37.9
General	7	y,z	.0197	284.0
General	9	y,z	.0086	206.0

However, once past this limit, the damping improvement is less drastic and the natural frequency of the coupled system is affected, as seen in the top figure of the simulation. When the simulation was reaccomplished using lower gains, the damping increased slightly. This indicates a need for a certain amount of tuning of the feedback gains once an estimate is determined in order to ensure the maximum damping is being achieved. This is a current area of research at Ga Tech.

7. Experimental Work

The final goal of this research was to test the controller on an experimental testbed. The testbed shown in Fig. 7 was extended to a two flexible link macromanipulator, allowing multiple degrees of freedom of base flexibility. A disturbance was applied to the macromanipulator in each direction (x, y, and z) as well as a general disturbance. The dominant (lowest frequency) free vibration modes of the macromanipulator are at 1, 1.2, 4.2, 7, and 9.5 Hz with damping ratios of. 0.018 6, 0.006 7, 0.008 7, 0.005 13, and 0.002 81, respectively. Table 2 summarizes the resulting modes of vibration and damping ratios with vibration control.

The damping of the macromanipulator improved with the vibration controller in place, although many implementation issues arose that limited the effectiveness of the scheme on the testbed. This is an on-going area of research at Georgia Tech.

8. Conclusions

This paper presented research in developing a control scheme to provide position control and enhanced vibration damping of a macro/micro-manipulator. The configuration of a rigid manipulator attached to a flexible base was introduced as a similar configuration. The system model was described along with the interaction forces and torques, which vary throughout the workspace. This variation

in performance may be used to choose joint configurations better suited for inertial damping. In addition, guidelines on choosing vibration controller feedback gains were established. Simulation and experimental results were presented demonstrating the effectiveness of the control scheme in damping vibration. More detail on all of this work may be found in Ref. (9).

Acknowledgements

Partial funding for this work was provided by the Air Force Institute of Technology U.S. Air Force Academy Faculty Preparation Program and the HUSCO/Ramirez Endowed Chair for Fluid Power and Motion Control.

Disclaimer

The views expressed in this article are those of the authors and do not reflect the official policy or position of the United States Air Force, Department of Defense, or U.S. Government.

References

(1) Book, W. and Loper, J., Inverse Dynamics for Commanding Micromanipulator Inertial Forces to Damp Macromanipulator Vibration, Proc. IEEE Robot Society of Japan International Conf. on Intelligent Robots and Systems, Vol. 2 (1999), pp. 707-714.

(2) Torres, M. and Dubowsky, S., Path Planning for Elastically Constrained Space Manipulator Systems, Proc. IEEE International Conf. on Robotics and Automation, Vol. 1 (1993), pp. 812-817.

(3) Senda, K., Dynamics and Control of Rigid/Flexible Space Manipulators, Ph.D. Thesis, University of Osaka Prefecture, Sakai, Osaka, (1993).

(4) Singhose, W., Singer, N. and Seering, W., Comparison of Command Shaping Methods for Reducing Residual Vibration, Proc. 3rd European Control Conf., Vol. 2 (1995), pp. 1126-1131.

(5) Lew, J. and Moon, S.-M., A Simple Active Damping Control for Compliant Base Manipulators, IEEE/ASME Transactions on Mechatronics, Vol. 2 (2001), pp. 707-714.

(6) Sharf, I., Active Damping of a Large Flexible Manipulator with a Short-Reach Robot, Proceedings of the 1995 American Control Conference, Seattle, WA, Vol. 5, June 21-23, (1995), pp. 3329-3333.

(7) Book, W., Recursive Lagrangian Dynamics of Flexible Manipulator Arms, The International Journal of Robotics Research, Vol. 3, No. 3 (1993), pp. 87-100.

(8) Sciavicco, L. and Siciliano, B., Modeling and Control of Robot Manipulators, (2000), pp. 151-162, McGraw-Hill, New York.

(9) George, L., Active Vibration Control of a Flexible Base Manipulator, Ph.D. Thesis, Georgia Institute of Technology, Atlanta, GA, (2002).

(10) Book, W. and Lee, S.H., Vibration Control of a Large Flexible Manipulator by a Small Robotic Arm, Proc. of the American Control Conf., Vol. 12 (1989), pp. 1377-1380.